

Long-term variations of wind and wave conditions in the coastal regions of the Black Sea

Adem Akpınar¹ · Bilal Bingölbali¹

Received: 27 March 2016 / Accepted: 23 May 2016 / Published online: 30 May 2016
© Springer Science+Business Media Dordrecht 2016

Abstract Spatial and temporal variations of significant wave height (H_{m0}) and wind speed (WS) at selected locations over the Black Sea are studied based on 31-year long-term SWAN simulations forced with Climate Forecast System Reanalysis dataset. The objective was to investigate whether or not there is a possible increase in wind and wave conditions along the Black Sea shelves. Wind and wave parameters are obtained at 33 locations enclosing the Black Sea coast line from SWAN simulations and annual mean and maximum H_{m0} and WS values as the climatological variables are computed for these locations. Using these data, long-term trends and their significance at these locations are investigated based on Mann–Kendall trend test. To quantify the trends, Sen’s slope estimator and least square linear regression (the slope of the linear best-fit curve) are used. Variation of monthly mean H_{m0} and WS values at these locations are also discussed. Besides, decadal variations of these four climatological variables at 33 locations are studied. The results show that higher wind speeds and wind wave heights are monitored in the winter season in all locations, while during the summer months, there is a significant drop in both H_{m0} and WS. In the western Black Sea, average H_{m0} is highest (about 1.02 m) at locations 23 and 25. During the period of 1979 and 2009, it is determined that mean WS has a weak significant increasing trend (maximum 1.29 cm/s/year) along the north-eastern coasts of Turkey and the Crimean peninsula, while there is no statistically significant H_{m0} trend in the Black Sea except at location 11, offshore Sochi in the north-eastern part of the Black Sea. A weak decreasing trend (maximum 0.24 cm/year) in mean H_{m0} is seen along the north-western coasts of Turkey, while maximum H_{m0} and WS show no statistically significant increasing or decreasing trend except location 2, which has a weak significant increasing trend for maximum WS. All the trends at other locations for four variables are statistically insignificant, and they have no trend. The most significant difference is observed in maximum WS as 6.14 m/s in different decades in the north-western part of the Black Sea. The difference in the decades is very low in mean H_{m0} at all locations. Mean

✉ Adem Akpınar
ademakpinar@uludag.edu.tr

¹ Department of Civil Engineering, Uludağ University, Gorukle Campus, Bursa, Turkey

wind and wave conditions at all locations have almost negligible difference, whereas decadal variations of maximum H_{m0} and WS show high differences. This may be probably due to storms and cyclones conditions.

Keywords Trend · Significant wave height · Wind speed · SWAN model · Black Sea

1 Introduction

In situ measurements, voluntary observing ships data, satellite altimeter, and model simulations are generally used to assess wind and wave climate in any region. In most regions of the world, in situ measurements are sparse, and they are also not available for a long period for an accurate assessment of wind and wave climate in these areas. It should be noticed that for wind and wave climatologists, accuracy and duration of the wave data without significant gaps are of a great importance. Although for coastal engineering applications, wave measurements of a minimum 1-year time period are used, wind and wave measurements of at least a period of 10 years or even 30 years are required to yield reliable information on wave climate or extreme wave statistics (Swain 1997). Data from voluntary observing ships have always been of great importance since 1784, but Soares (1986) stated that visual wind and wave observations from ships need to be calibrated with buoy measurements. Besides, such measurements are made along the ship routes and they are subjective. Moreover, large un-sampled areas over the oceans are available due to missing ship routes (Gulev and Grigorieva 2004). Satellite altimetry along with its recent improvement in data quality and resolution is also preferred to discover wind and wave characteristics, but these data miss the chances in extreme events. Therefore, trends and variability of severe wave events and wave climate were analyzed by using numerical wave model hindcasts. Existing observations have also been complemented with these model results used as a common tool (e.g., Sterl et al. 1998; Wang and Swail 2002). Finally, the calibrated and validated wave reanalysis data forced with the modeled and measured oceanic wind fields can contribute to increase in the available observations. The effect of wind and wave variability and evaluations of possible cause can also be investigated with these reanalysis data (Wolf and Woolf 2006). The global reanalysis data have some advantages, e.g., their physical consistency and relatively high temporal coverage. Although their coarse spatial resolution causes some limitations in the use of such data in regional climate studies, inhomogeneity is not conceived as a problem (WASA Group 1998; Shanas and Kumar 2015). In this study, we therefore used 31-year long-term SWAN model hindcasts forcing with the Climate Forecast System Reanalysis (CFSR) reanalysis.

Significant trends in the winds and wind waves in different seas in the world were reported by several authors (Bacon and Carter 1990; Gulev and Hasse 1999; Sterl et al. 1998; Grevemeyer et al. 2000; Wang and Swail 2001; Cox and Swail 2001; Gower 2002; Woolf et al. 2002; Mendez et al. 2006, 2008; Dragani et al. 2010; Kumar and Sajiv 2010; Sajiv et al. 2012; Kumar et al. 2013; Shanas and Kumar 2015; Hithin et al. 2015; Anoop et al. 2015; Kumar and Anoop 2015).

Wave climate is highly variable on the world's coast, and its temporal changes and extremes usually imply consequences like erosion or impacts to infrastructures. It is well known that variations in wave climate may cause extensive coastal impacts (Reguero et al. 2013). Therefore, an understanding of wind and wave climate and their long-term

variations in any region is an important issue. To the authors’ knowledge, the decadal variations and long-term changes in the winds and wind waves in the Black Sea region have not been investigated. Trend analysis in this area has also not been applied yet. Therefore, the main purpose of our study is to quantify long-term trends, the inter-annual variability, and decadal variations of the winds and wind waves simulated for 31 years for the selected locations in the Black Sea. In the current study, the mean and maximum values of wind speeds (WS) and significant wave heights (H_{m0}) were used as climatological variables to determine long-term changes.

Quantifying the significance of trends in hydro-meteorological time series has been frequently performed by using the Mann–Kendall statistical test (Douglas et al. 2000; Wang and Swail 2001, 2002; Cairns et al. 2004; Partal and Kahya, 2006; Tabari et al. 2011). The slope value in hydro-meteorological time series has also widely been computed by using the Sen’s slope estimator and linear regression (Wang and Swail 2002; Yue and Hashino 2003; Partal and Kahya 2006; Tabari and Marofi 2011; Vanem and Walker 2013). Therefore, we used these trend methods to detect long-term trends of the climatological parameters in the Black Sea.

This paper is focused on studying the trends in the annual means and maximums in wind and wave conditions computed from a 31-year numerical simulation carried out with

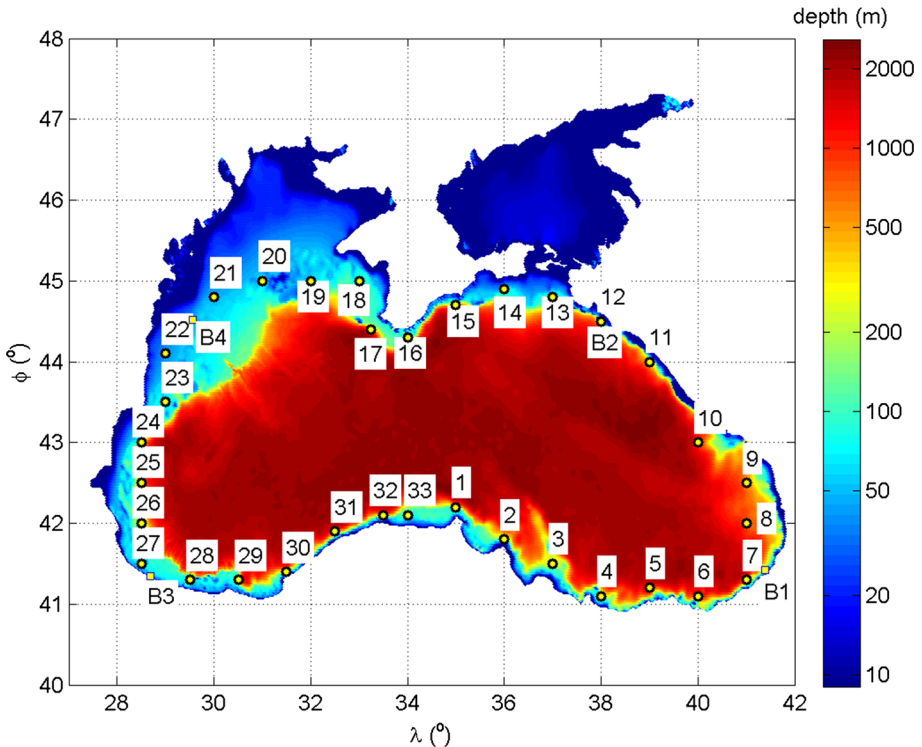


Fig. 1 Study area, computational domain where SWAN model was implemented, and bathymetry. The locations where modeled wave heights were studied are pointed out with *circles filled with yellow color*. Buoy positions, which are pointed out with *squares filled with yellow color*, are B1: Hopa, B2: Gelendzhik, B3: Karaburun, and B4: Gloria

SWAN model forced by the NCEP CFSR re-analysis along shelves of the Black Sea. The paper is organized as follows: Sect. 2 describes the materials and methods used in the study. Section 3 contains a discussion of the results, including model performance, variations in monthly mean H_{m0} and WS, and long-term and decadal variations in annual mean and maximum H_{m0} and WS, and Sect. 4 summarizes the conclusions.

Table 1 Positions of the locations studied, their water depths, and mean and maximum values of significant wave height (H_{m0}) and wind speed (WS) during 31 years at the locations studied

Location	Position (°)		H_{m0} (m)		WS (m/s)		Water depth (m)
	N	E	mean	max	mean	max	
1	42.2	35.00	0.87	5.98	4.82	21.39	160
2	41.8	36.00	0.70	4.98	3.61	18.68	186
3	41.5	37.00	0.73	5.34	4.18	22.87	205
4	41.1	38.00	0.58	4.46	3.83	18.81	520
5	41.2	39.00	0.67	5.72	3.64	18.12	1258
6	41.1	40.00	0.60	5.53	3.35	17.08	936
7	41.3	41.00	0.56	5.04	3.61	17.01	1390
8	42.0	41.00	0.74	7.18	4.94	23.59	1445
9	42.5	41.00	0.71	6.18	4.84	19.87	1287
10	43.0	40.00	0.77	5.92	5.08	21.80	1400
11	44.0	39.00	0.72	5.51	5.14	23.20	294
12	44.5	38.00	0.61	6.19	4.93	24.33	178
13	44.8	37.00	0.83	6.49	6.41	24.37	237
14	44.9	36.00	0.77	5.92	5.97	24.17	59
15	44.7	35.00	0.63	5.78	4.71	21.21	526
16	44.3	34.00	0.77	6.51	5.08	24.52	96
17	44.4	33.25	0.88	7.36	5.84	26.78	886
18	45.0	33.00	0.75	7.08	5.72	27.19	94
19	45.0	32.00	0.95	6.75	6.44	28.34	59
20	45.0	31.00	1.01	6.27	6.67	28.91	59
21	44.8	30.00	0.95	6.21	6.43	26.69	43
22	44.1	29.00	0.91	6.12	6.26	24.74	44
23	43.5	29.00	1.02	7.22	6.52	26.85	84
24	43.0	28.50	0.97	7.28	6.13	25.63	91
25	42.5	28.50	1.02	7.57	6.27	25.93	547
26	42.0	28.50	1.01	7.91	6.10	24.38	91
27	41.5	28.50	0.86	7.57	4.94	21.13	67
28	41.3	29.50	0.90	8.71	5.04	21.40	71
29	41.3	30.50	0.87	8.29	4.65	19.42	336
30	41.4	31.5	0.68	6.89	3.88	17.25	245
31	41.9	32.5	0.85	6.15	4.97	22.78	921
32	42.1	33.5	0.82	5.51	4.38	19.12	608
33	42.1	34.0	0.79	5.43	4.08	19.28	92

2 Materials and methods

2.1 The study area and the locations studied

The Black Sea is the largest confined basin of the world (Özsoy and Ünlüata 1997) with an aquatic surface of 0.4 million km² and a total volume of 0.55 million km³. The bathymetry (Fig. 1) extends to depths of 2200 m, with an average depth 1200 m, and is characterized by steep topography near the coastline, especially for the south-eastern part of the domain. The continental shelf spreads mainly in the northwestern and western parts of the Black Sea, along the coastal zones of Bulgaria, Romania, and Ukraine (Krestenitis et al. 2012). Thirty-three locations along these coastal regions of the Black Sea are selected for the study considering approximately 1 degree spacing in longitude of the locations. Among these 33 locations, nine locations (1–9) are in the south-eastern, seven locations (10–16) in the north-eastern, eight locations (17–24) in the north-western, and nine locations (25–33) in the south-western parts of the Black Sea. The positions of these locations are illustrated in Fig. 1, and their coordinates, water depths, and mean and maximum values of H_{m0} and WS simulated during 31 years at the locations studied are given in Table 1. The locations studied are in water depth more than 40 m (Table 1). Based on Table 1, the highest value of mean H_{m0} (1.02 m) is simulated at both locations 23 and 25, while the lowest mean H_{m0} (0.83 m) is at location 13. Maximum H_{m0} has the highest value (8.71 m) at location 28, while having its lowest value (6.51 m) at location 16. Mean WS shows a highest value (6.67 m/s) at location 20, while showing a relatively low value (4.94 m/s) at location 8. And finally, maximum WS's highest value (28.91 m/s) is simulated at location 20, and its lowest value (23.59) is at location 8. It is seen that the locations of highest and lowest wind speeds are not similar to those of significant wave height.

2.2 The model applied

Wind and wave parameters in the Black Sea were calculated during 31 years by using a third-generation wave model, SWAN (Ris et al. 1999; Booij et al. 1999) for the locations studied. For the calculation of wave parameters on various scales, this model is widely used all over the world (e.g., Rusu et al. 2008; Van Ledden et al. 2009; Zijlema 2010; Gorrell et al. 2011). It was also implemented in several Black Sea studies (e.g., Polonsky et al. 2011; Akpınar et al. 2012; Valchev et al. 2012; Van Vledder and Akpınar 2015). In this study, the SWAN cycle III version 41.01 model was used to perform the hindcast study. It was run in the third generation and non-stationary mode with a time step equal to 15 min and one iteration per time step, as was found to be sufficient (Akpınar et al. 2012) to accurately predict the wave conditions in the Black Sea. The model domain covers the entire Black Sea, from 27°E to 42°E of longitude and from 40°N to 48°N of latitude shown in Fig. 1. The domain was discretized with a regular grid of 225 × 120 nodes in spherical coordinates with a uniform resolution of 0.067° (1/15°) in each direction. The directional wave energy density spectrum function was discretized using 36 directional bins and 35 frequency bins between 0.04 and 1.0 Hz. The numerical scheme was the slightly dispersive BSBT (first-order upwind; backward in space, backward in time) scheme. Details regarding the numerical settings of the SWAN model in the Black Sea can be found in Akpınar et al. (2012).

For our wave model computations, we have used the calibrated SWAN model (Akpınar et al. 2015): for whitecapping, the expression by Janssen (1989, 1991) is used, in which

delta = 1 according to Rogers et al. (2003), and coefficient for determining the rate of whitecapping dissipation (C_{ds}) equals to 1.5; for wind, the formulation of Komen et al. (1994) is used. Quadruplet interactions are estimated using the discrete interaction approximation (DIA) by Hasselmann et al. (1985) using $\lambda = 0.25$ and $C_{n4} = 3 \times 10^7$. The JONSWAP bottom friction formulation is used with $C_{fjon} = 0.038 \text{ m}^2\text{s}^{-3}$ according to Zijlema et al. (2012). Depth-limited wave breaking is modeled according to the bore model of Battjes and Janssen (1978) using $\alpha = 1$ and $\gamma = 0.73$. The triad wave–wave interactions using the lumped triad approximation (LTA) of Eldeberky (1996) in the SWAN were also activated. We applied the refraction limiter with $C_{THETA} = 0.5$ to avoid local instabilities that would otherwise spread through the domain (Dietrich et al. 2012).

2.3 Data used

The SWAN model was forced by the CFSR wind fields (Saha et al. 2010) from the National Centers for Environmental Prediction (NCEP). The CFSR was designed and executed as a global, high-resolution, coupled atmosphere–ocean–land surface–sea ice system to provide the best estimate of the state of these coupled domains over the period of 31 years from 1979 to 2009. Temporal resolution of the CFSR wind fields is 1 h. They have also 0.3125° spatial resolution both latitude and longitude. The other input for the SWAN model was the bathymetric data obtained from GEBCO (2014), General Bathymetric Charts of the Ocean, produced by the British Oceanographic Data Centre (BODC) at a resolution of 30 arc-seconds in both latitude and longitude. It is shown in Fig. 1 as a contoured map for the study area.

For validation of the SWAN model, the measured data at four locations over the Black Sea were used. The first location was the Hopa buoy ($41^\circ 25' 24''$ N, $41^\circ 23' 00''$ E, denoted to B1 in Fig. 1) located in deep water (100 m). Gelendzhik buoy (denoted to B2 in Fig. 1), the second location, was located at $44^\circ 30' 27''$ N, $37^\circ 58' 42''$ E in deep water (85 m). At both locations, the measurements were obtained by the Datawell Directional Waverider buoy. Data for 1999 and 2001 at Hopa and Gelendzhik, respectively, were provided within the NATO TU-WAVES project (Özhan and Abdalla 1998). The third measurement location was Karaburun ($41^\circ 21' 0.869''$ N, $28^\circ 41' 27''$ E, denoted to B3 in Fig. 1) located in a water depth of 16 m. Data, which were measured by the Wave Observer, for 2004 at this location were provided from Çevik et al. (2006), Şahin (2007), and Batu (2008). Gloria drilling platform ($44^\circ 31' 1''$ N, $29^\circ 34' 1''$ E, denoted to B4 in Fig. 1) located in a water depth of about 50 m was the last location. Data, which were measured by non-directional wave gages, for 2008 at this location were provided from the NIMRD (Oceanography Department).

2.4 Methods used

Significant trends in H_{m0} and WS time series can be tested using parametric and non-parametric methods. Data used in parametric trend tests are independent and normally distributed, while in nonparametric trend tests, they are only independent. In this study, Mann–Kendall, a nonparametric trend test, is used to detect H_{m0} and WS trends. The test statistic (S) in Mann–Kendall test (Mann 1945; Kendall 1975) is given as below:

$$S = \sum_{i=1}^{n-1} \sum_{j=i+1}^n \text{sgn}(x_j - x_i) \tag{1}$$

where n , x_i , and x_j are, respectively, the number of data and the data values in time series i and j ($j > i$). $\text{sgn}(x_j - x_i)$ is a sign function which is given as below:

$$\text{sgn}(x_j - x_i) = \begin{cases} +1 & \text{if } (x_j - x_i) > 0 \\ 0 & \text{if } (x_j - x_i) = 0 \\ -1 & \text{if } (x_j - x_i) < 0 \end{cases} \tag{2}$$

The variance of S is calculated as below:

$$\text{Var}(S) = \frac{n(n-1)(2n+5) - \sum_{i=1}^m t_i(t_i-1)(2t_i+5)}{18} \tag{3}$$

where m and t_i are the number of tied groups and ties of extent i , respectively. A set of sample data having the same value represent a tied group. If the sample size $n > 10$, the standard normal test statistic (Z_s) given below is used.

$$Z_s = \begin{cases} \frac{S-1}{\sqrt{\text{Var}(S)}}, & \text{if } S > 0 \\ 0 & \text{if } S = 0 \\ \frac{S+1}{\sqrt{\text{Var}(S)}}, & \text{if } S < 0 \end{cases} \tag{4}$$

The null hypothesis where it is of no trend is rejected when $|Z_s| > Z_{1-\alpha/2}$. And it concludes that in the time series of wind and wave parameters, a significant trend of a specific significance level (α) is available. If the null hypothesis is accepted, it means there is no trend. Significance levels $\alpha = 0.01$ and $\alpha = 0.05$ are frequently used in such analysis. $Z_{1-\alpha/2}$ is obtained from the standard normal distribution table. As in the table, the null hypothesis is rejected if $|Z_s| > 1.96$ at 5 % significance level and rejected if $|Z_s| > 2.576$ at 99 % confidence interval $(1 - \alpha)$. If $|Z_s| < 1.96$ at the 5 % significance level, the null hypothesis of no trend is accepted. If the null hypothesis is rejected, increasing and decreasing trends for the associated parameters (H_{m0} and WS in this study) are determined based on the sign of Z_s . There is an increasing trend if the sign of Z_s is positive. Otherwise, a decreasing trend exists if the sign of Z_s is negative.

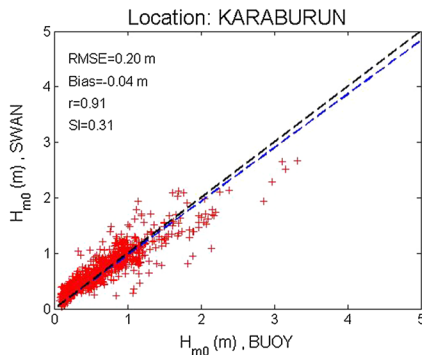
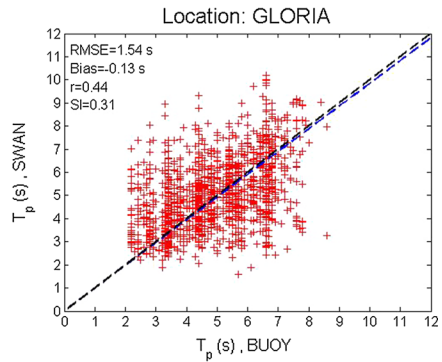
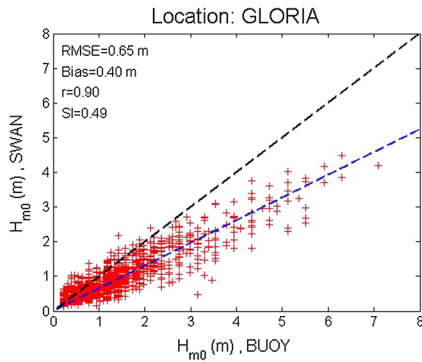
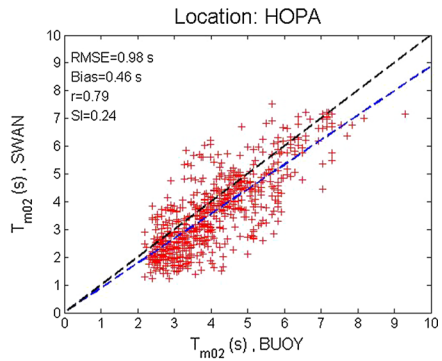
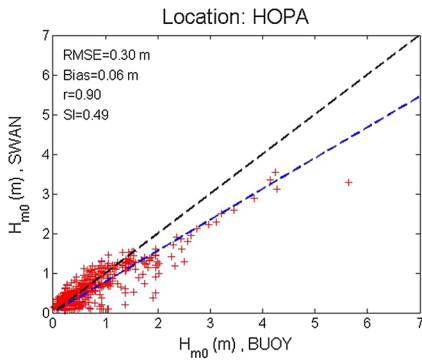
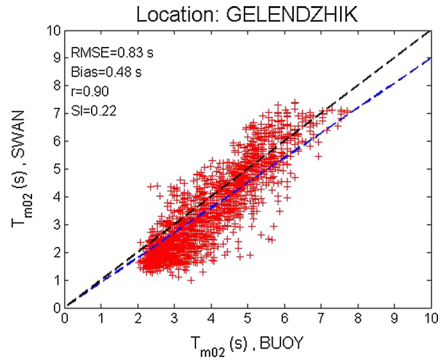
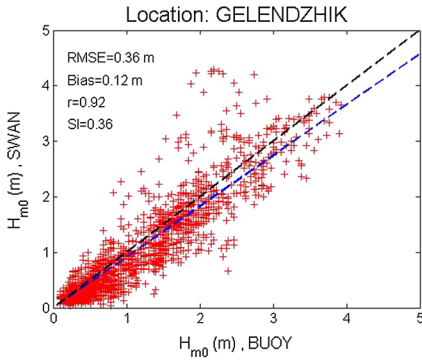
For estimating of the slope of trend, here a nonparametric procedure (Sen 1968) is used. According to this method, the slopes (Q_i) in the sample of N pairs of data are computed as below:

$$Q_i = \frac{x_j - x_k}{j - k} \quad \text{for } i = 1, \dots, N \tag{5}$$

where x_j and x_k represent the data values at times j and k ($j > k$), respectively.

The Sen’s slope estimator is the median of these N values of the slopes (Q_i). After the N values of Q_i are ranked from smallest to largest, it is computed as below:

$$Q_{\text{med}} = \begin{cases} Q_{[\frac{N+1}{2}]}, & \text{if } N \text{ is odd} \\ \frac{Q_{[\frac{N}{2}]} + Q_{[\frac{N+2}{2}]}}{2}, & \text{if } N \text{ is even} \end{cases} \tag{6}$$



◀ **Fig. 2** Scatter plots comparison of measured significant wave height (H_{m0}) and mean wave period (T_{m02}) or peak wave period (T_p) with SWAN simulation results including statistical error parameters at four measurements locations deployed in south-eastern, south-western, north-eastern, and north-western coasts (for 2001 at Gelendzhik, 1999 at Hopa, 2008 at Gloria, and 2004 at Karaburun)

The Q_{med} is the steepness of the trend, and its sign reflects data trend reflection. Finally, the trends of H_{m0} and WS are estimated based on Mann–Kendall trend test and Sen’s slope estimator. The slope of the linear best-fit line to the annual mean and maximum H_{m0} and WS during 31 years is computed to determine the trend.

Wave model performance is quantified by computing statistical parameters of predicted and measured H_{m0} and T_{m02} at the buoy locations. The following statistical parameters are used:

$$r = \frac{\sum_{i=1}^N ((P_i - \bar{P})(O_i - \bar{O}))}{\left[\left(\sum_{i=1}^N (P_i - \bar{P})^2 \right) \left(\sum_{i=1}^N (O_i - \bar{O})^2 \right) \right]^{1/2}} \tag{7}$$

$$\bar{P} = \frac{1}{N} \sum_{i=1}^N P_i \tag{8}$$

$$\bar{O} = \frac{1}{N} \sum_{i=1}^N O_i \tag{9}$$

$$RMSE = \left[\frac{1}{N} \sum_{i=1}^N (P_i - O_i)^2 \right]^{1/2} \tag{10}$$

$$SI = \frac{RMSE}{\bar{O}} \tag{11}$$

$$bias = \sum_{i=1}^N \frac{1}{N} (P_i - O_i) \tag{12}$$

where O_i and P_i are the observed and predicted values, \bar{O} and \bar{P} are the mean values of the observed and predicted data, and N is the total number of data. The Pearson correlation coefficient (r) shows the degree of the linear correlation (dependence) between two variables (predicted and observed data). If r value is closer to 1.0, it means that most points are placed on the straight regression line. If the parameters RMSE and SI are closer to 0.0, it shows that the model performance is very well. The mean bias parameter is defined as the mean of differences between predicted and observed values. Zero bias is called unbiased.

3 Results and discussion

3.1 Model performance

The SWAN model used in this study was developed, calibrated, and validated within a research project (Akpınar et al. 2015). Here, as an example, we present a comparison of SWAN simulation results with the measured data at buoy locations shown in Fig. 1 for

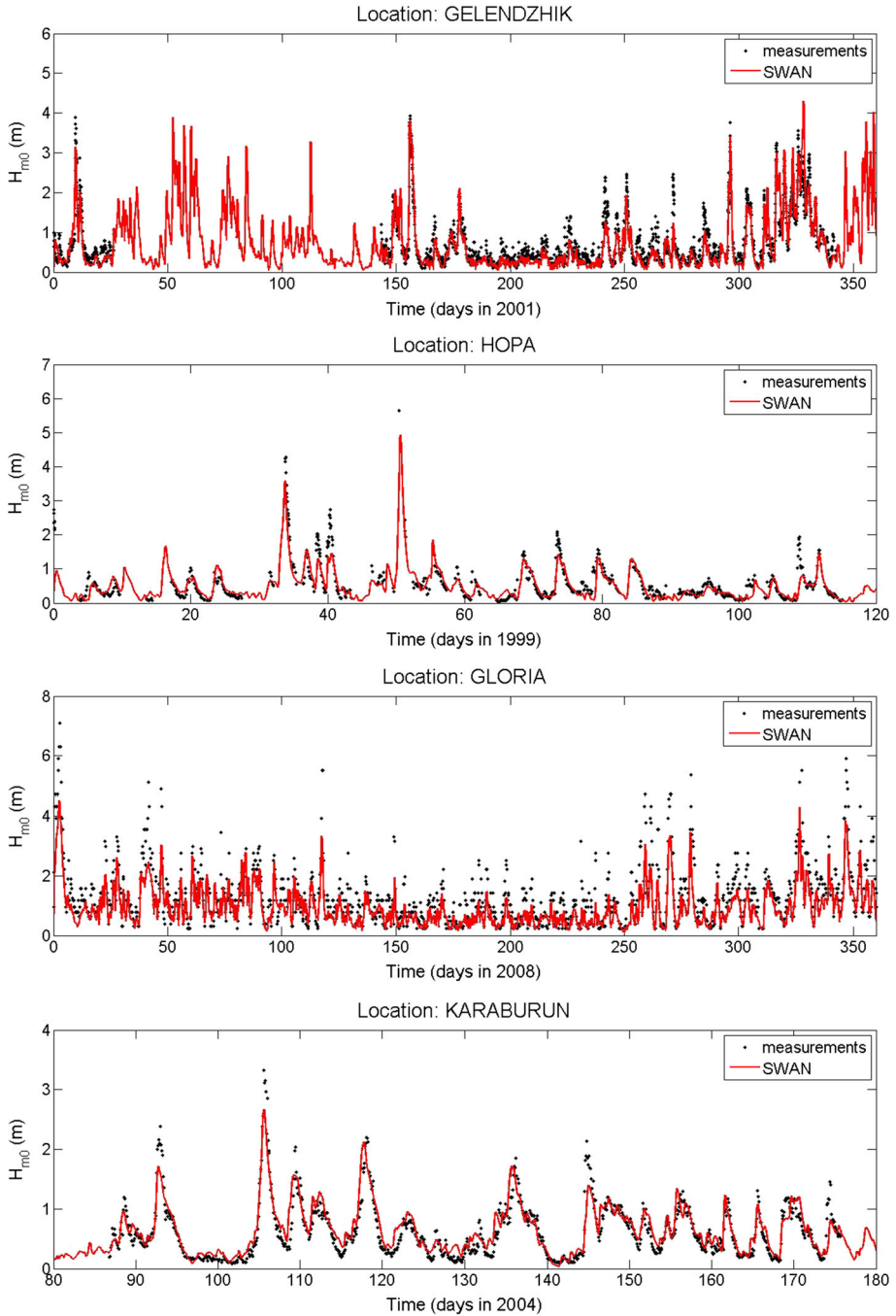


Fig. 3 Time series comparison of significant wave height (H_{m0}) from SWAN simulation results against the measured data for 2001 at Gelendzhik, 1999 at Hopa, 2008 at Gloria, and 2004 at Karaburun

validation of the SWAN model. Scatter plots comparison of measured H_{m0} and T_{m02} (or T_p) with SWAN simulation results at four measurements locations deployed in south-eastern, south-western, north-eastern, and north-western coasts are given in Fig. 2. It also presents statistical error parameters between the measured and simulated data. Time series comparison of SWAN and measured data are also shown in Fig. 3 for H_{m0} and Fig. 4 for T_{m02} . Scatter plots at Gelendzhik indicate that SWAN data are in good agreement with measured data for both H_{m0} and T_{m02} . For H_{m0} , the correlation coefficient is 0.92 with bias value of 0.12 m and scatter index of 36 %. The period at this location has a correlation coefficient of 0.90 with bias value of 0.48 s and scatter index of 22 %. At Gloria, SWAN data show a good agreement with measured data for the peak period (T_p) with $r = 0.90$, bias value of 0.40 m, and SI = 49 %. The SWAN model underestimated the H_{m0} at this

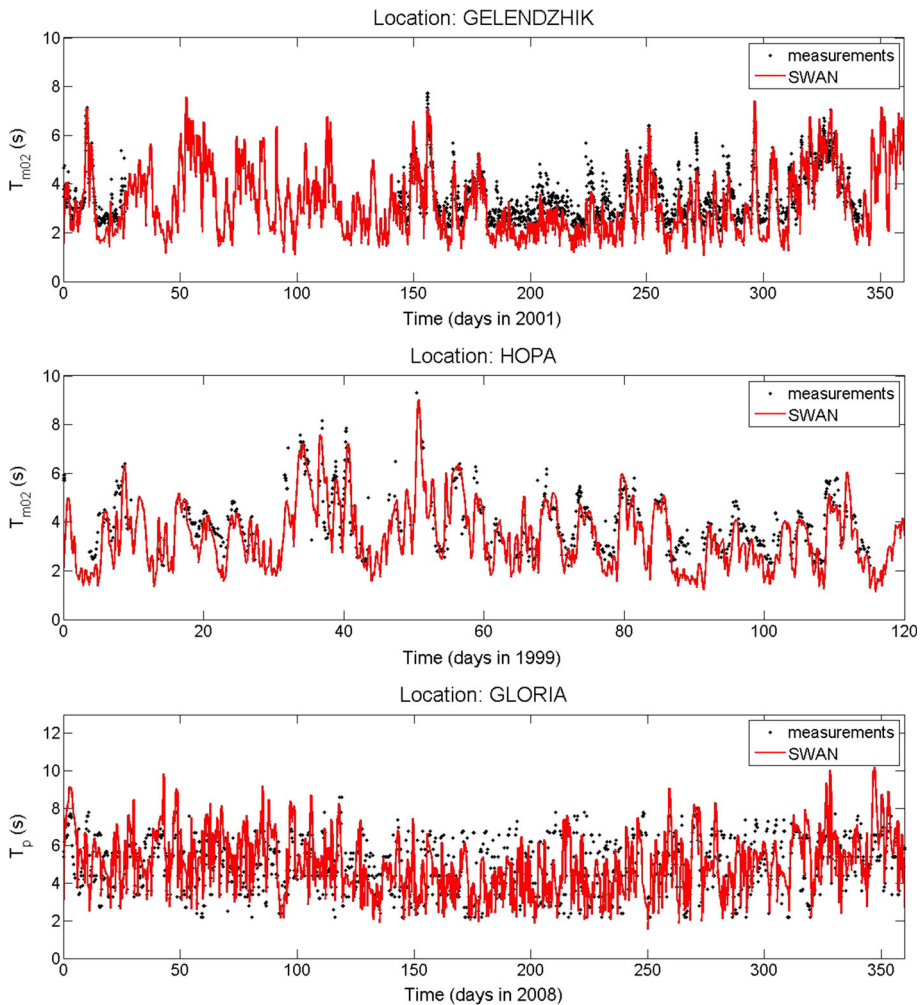


Fig. 4 Time series comparison of mean wave period (T_{m02}) and peak wave period (T_p) from SWAN simulation results against the measured data for 2001 at Gelendzhik, 1999 at Hopa, 2008 at Gloria, and 2004 at Karaburun

location for high values. Scatter plots at Hopa in 1999 also show an agreement of SWAN with measured data in both H_{m0} and T_{m02} . For T_{m02} , r and bias values are 0.79 and 0.46 s, while the scatter index and RMSE are 24 % and 0.98 s, respectively. The H_{m0} at Hopa has a correlation coefficient of 0.90 with the bias value of 0.06 m, the scatter index of 49 %. Due to lack of the measured period data in our hands at Karaburun, only H_{m0} at this location is examined and its statistical error values are given as follows; $r = 0.90$, bias = -0.04 m, RMSE = 0.20 m, and SI = 31 %. As can be seen from these results, Gloria has the highest RMSE (0.65 m) and bias (0.40 m) values for H_{m0} , while Karaburun has the lowest RMSE (0.20 m) and bias (-0.04 m) values. For T_{m02} , the lowest (RMSE = 0.83 s and SI = 0.22) and highest (RMSE = 1.54 s and SI = 0.31) errors were obtained at Gelendzhik and Gloria, respectively. As these results, it can be concluded that the SWAN model performs rather well. However, it is also observed that the model has worse quality at Gloria (B4) in comparison with other locations. Therefore, it is also concluded that the conclusions in that region are not as accurate as the other parts. In this study, a 31-year simulation was performed using the SWAN model forced with the CFSR winds. Some wind and wave parameters were obtained as the outputs at 33 locations over the Black Sea during 31 years. These outputs were used in the analyses below.

3.2 Variations in monthly mean H_{m0} and WS

Monthly mean H_{m0} and WS values were computed from 31-year SWAN simulation at all locations (location nos. 1–33) studied along the Black Sea shelves. For locations (1–9) placed in the south-eastern part of the Black Sea, variations of monthly mean H_{m0} are shown in upper left panel of Fig. 5. This shows that during the winter months of November to February, the monthly mean H_{m0} is highest (1.15 m) in December and January at location 1 in this region. During the summer season (April–September), the monthly mean H_{m0} decreases at all locations. The lowest H_{m0} value (0.4 m) is observed in June at location 4. Monthly mean WS values were also computed from 31-year SWAN simulation

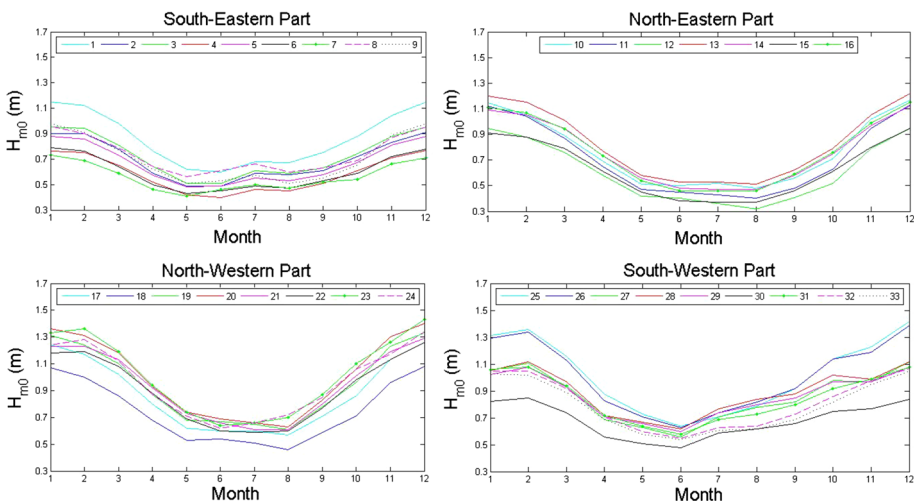


Fig. 5 Variations in monthly mean H_{m0} computed from 31-year SWAN simulation at locations studied along the Black Sea shelves

at all locations studied along the Black Sea shelves. For locations (location nos. 1–9) placed in the south-eastern part of the Black Sea, variations of monthly mean WS are shown in upper left panel of Fig. 6. As can be seen, in this region, mean WS has the highest value (6.47 m/s) in December at location 9, while the lowest WS value (2.78 m/s) is observed in August at location 6.

Along the north-eastern side of the Black Sea at locations 10–16, H_{m0} is higher during the months of November to February with highest mean H_{m0} (1.22 m) in December at location 13 (in upper right panel of Fig. 5). At this location, it has higher values for the all of the other months in comparison with other locations. The lowest H_{m0} (0.32 m) is found in August at location 12. Locations 12 and 15 have the lowest H_{m0} values during the all months. Looking at mean WS for this region (in upper right panel of Fig. 6), the highest (7.88 m/s) is in December at location 13, while the lowest (3.65 m/s) is in July at location 10. It can be seen that higher winds produce larger waves at location 13. In the north-western part of the Black Sea, location 23 has the highest mean H_{m0} (1.43 m) in December in this region, which is also the highest mean H_{m0} among the rest recorded in the other regions. Its lowest H_{m0} is 0.46 m at location 18 in August. Location 23 has also the highest WS (8.16 m/s) in December and the lowest (4.63 m/s) at location 18 in August. In this region, the highest H_{m0} and WS were seen during all months in comparison with other three parts. In the south-western part of the Black Sea, a maximum H_{m0} value of 1.42 m was seen in December and in June at location 25, and it has its lowest value (0.48 m) at location 30. Its highest mean WS is 7.85 m/s at location 25, and its lowest mean WS is 3.62 m/s at the same location in May.

3.3 Long-term variation in annual mean and maximum H_{m0} and WS

In this section, the trend in wave climate and wind behavior at selected locations over the Black Sea from 1979 to 2009 is studied. The Mann–Kendall test, Sen’s slope estimator, and the slope of the linear best-fit curve to the annual data of the selected parameters for

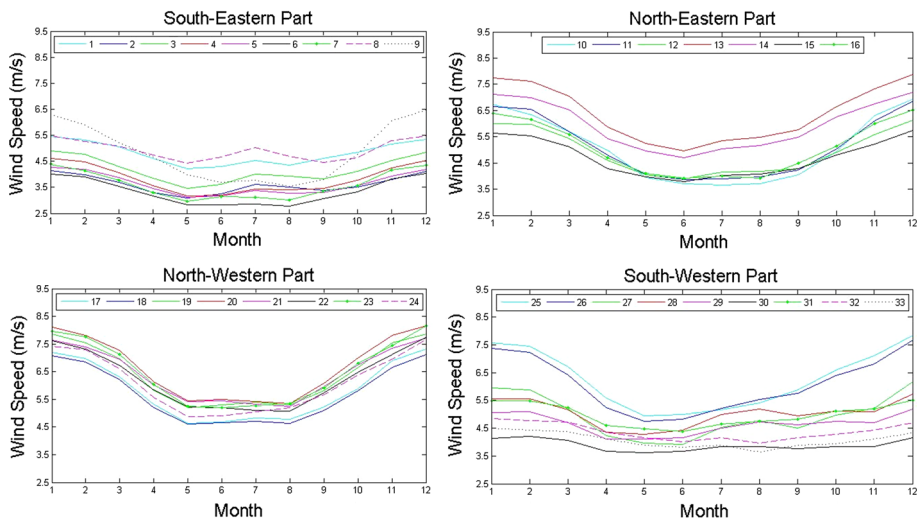


Fig. 6 Variations in monthly mean WS computed from 31-year SWAN simulation at locations studied along the Black Sea shelves

31 years were applied to the time series 1979–2009 for the four variables, namely mean and maximum H_{m0} and WS.

The results based on Mann–Kendall test, the Sen’s slope estimator, and the slope of the linear best-fit curve to the annual mean and maximum H_{m0} and WS for 31 years are given in Tables 2, 3, 4, and 5. For mean H_{m0} , a weak increasing trend was seen at locations 10–18, while there is a weak decreasing trend at locations 26–31. At all other locations, a

Table 2 Long-term trends in annual mean H_{m0} using Sen’s slope estimator and linear regression methods

Location	Test Z	Sen estimator		Linear regression		Trend	
		Q (cm/s)	B	Q (cm/s)	B	at $\alpha = 0.05$	at $\alpha = 0.01$
1	0.44	0.054	0.85	0.053	-0.19	No trend	No trend
2	0.20	0.012	0.69	0.022	0.26	No trend	No trend
3	1.09	0.066	0.72	0.089	-1.04	No trend	No trend
4	0.41	0.035	0.58	0.027	0.05	No trend	No trend
5	1.26	0.089	0.66	0.085	-1.02	No trend	No trend
6	1.19	0.081	0.58	0.084	-1.08	No trend	No trend
7	1.22	0.086	0.54	0.094	-1.30	No trend	No trend
8	1.67	0.137	0.70	0.136	-1.98	No trend	No trend
9	1.12	0.085	0.69	0.099	-1.27	No trend	No trend
10	1.50	0.879	4.93	0.186	-2.94	No trend	No trend
11	2.31	0.300	0.67	0.370	-6.66	Increasing trend	No trend
12	1.84	0.233	0.59	0.290	-5.16	No trend	No trend
13	1.26	0.178	0.80	0.218	-3.52	No trend	No trend
14	1.22	0.131	0.81	0.177	-2.75	No trend	No trend
15	1.46	0.115	0.61	0.172	-2.80	No trend	No trend
16	1.02	0.109	0.75	0.161	-2.45	No trend	No trend
17	0.92	0.117	0.85	0.148	-2.07	No trend	No trend
18	1.36	0.164	0.71	0.165	-2.54	No trend	No trend
19	0.51	0.080	0.93	0.130	-1.64	No trend	No trend
20	-0.14	-0.009	1.01	0.054	-0.08	No trend	No trend
21	-0.17	-0.021	0.95	0.037	0.20	No trend	No trend
22	0.00	0.004	0.90	0.022	0.48	No trend	No trend
23	-0.27	-0.028	1.01	0.018	0.66	No trend	No trend
24	-0.24	-0.017	0.96	0.009	0.79	No trend	No trend
25	-1.09	-0.060	1.01	-0.038	1.78	No trend	No trend
26	-1.39	-0.168	1.03	-0.106	3.12	No trend	No trend
27	-1.84	-0.226	0.88	-0.171	4.28	No trend	No trend
28	-2.04	-0.292	0.93	-0.245	5.79	Decreasing trend	No trend
29	-2.21	-0.286	0.90	-0.247	5.80	Decreasing trend	No trend
30	-2.48	-0.227	0.71	-0.202	4.71	Decreasing trend	No trend
31	-2.24	-0.223	0.88	-0.195	4.74	Decreasing trend	No trend
32	-1.19	-0.103	0.83	-0.072	2.26	No trend	No trend
33	-0.41	-0.030	0.79	-0.028	1.34	No trend	No trend

Table 3 Long-term trends in annual maximum H_{m0} using Sen’s slope estimator and linear regression methods

Location	Test Z	Sen estimator		Linear regression		Trend	
		Q (cm/s)	B	Q (cm/s)	B	at $\alpha = 0.05$	at $\alpha = 0.01$
1	-0.24	-0.125	4.78	-0.446	13.66	No trend	No trend
2	-0.41	-0.570	3.92	-0.398	11.79	No trend	No trend
3	0.44	0.332	4.07	0.548	-6.76	No trend	No trend
4	0.95	0.763	3.04	0.885	-14.44	No trend	No trend
5	0.34	0.306	3.96	0.416	-4.14	No trend	No trend
6	-0.03	-0.038	3.60	-0.004	3.83	No trend	No trend
7	0.00	0.007	3.86	0.100	1.79	No trend	No trend
8	-1.12	-1.256	5.12	-0.732	19.47	No trend	No trend
9	-0.51	-0.646	3.93	-0.085	5.68	No trend	No trend
10	-0.24	-0.201	3.96	-0.321	10.41	No trend	No trend
11	0.24	0.407	4.44	0.423	-3.90	No trend	No trend
12	1.09	0.998	4.26	2.102	-37.48	No trend	No trend
13	0.88	1.723	4.66	1.850	-32.02	No trend	No trend
14	0.58	1.004	4.50	1.350	-22.68	No trend	No trend
15	0.48	0.862	3.40	1.329	-22.77	No trend	No trend
16	1.05	1.835	3.95	1.990	-35.27	No trend	No trend
17	0.00	0.096	4.64	-0.445	13.71	No trend	No trend
18	0.44	0.853	4.36	0.158	1.36	No trend	No trend
19	0.00	0.007	18.81	-0.453	13.78	No trend	No trend
20	-0.34	-0.541	4.70	-0.393	12.64	No trend	No trend
21	-0.61	-0.844	4.58	-1.321	31.04	No trend	No trend
22	-0.92	-2.302	4.95	-1.905	42.60	No trend	No trend
23	-1.16	-1.689	5.63	-1.808	41.37	No trend	No trend
24	-0.65	-1.375	5.72	-1.660	38.47	No trend	No trend
25	-0.20	-0.665	6.12	-1.328	32.40	No trend	No trend
26	-0.14	-0.162	6.23	-0.901	24.05	No trend	No trend
27	0.78	1.611	5.23	0.344	-1.32	No trend	No trend
28	0.00	-0.022	5.39	0.217	1.26	No trend	No trend
29	0.37	0.556	5.01	0.670	-8.14	No trend	No trend
30	0.31	0.387	3.89	0.950	-14.84	No trend	No trend
31	0.48	0.352	4.34	0.346	-2.33	No trend	No trend
32	-0.61	-0.728	4.24	-0.613	16.35	No trend	No trend
33	-0.48	-0.629	4.08	-1.244	28.84	No trend	No trend

very negligible trend was available (Table 2). Variation of long-term trend in wave climate and wind behavior is different for different locations. As the slope of the linear best-fit curve, the trends for both H_{m0} and WS in south-eastern region (locations 1–9) of the Black Sea show a weak increasing trend. In this region, mean H_{m0} has a maximum increasing trend of 0.136 cm/year at location 8 and a minimum increasing trend of 0.022 cm/year at

Table 4 Long-term trends in annual mean WS using Sen's slope estimator and linear regression methods

Location	Test Z	Sen estimator		Linear regression		Trend	
		Q (cm/s)	B	Q (cm/s)	B	at $\alpha = 0.05$	at $\alpha = 0.01$
1	0.99	0.389	4.77	0.398	-3.13	No trend	No trend
2	2.28	0.696	3.50	0.720	-10.74	Increasing trend	No trend
3	2.79	0.787	4.05	0.813	-12.04	Increasing trend	Increasing trend
4	0.82	0.764	4.37	0.534	-6.82	No trend	No trend
5	2.82	0.647	3.56	0.714	-10.59	Increasing trend	Increasing trend
6	2.52	0.654	3.26	0.718	-10.97	Increasing trend	No trend
7	1.02	0.330	3.57	0.453	-5.43	No trend	No trend
8	1.24	0.378	4.89	0.450	-4.05	No trend	No trend
9	-0.24	-0.197	4.86	0.009	4.66	No trend	No trend
10	1.50	0.879	4.93	0.930	-13.46	No trend	No trend
11	1.67	0.901	4.99	1.219	-19.17	No trend	No trend
12	0.71	0.415	4.88	0.469	-4.43	No trend	No trend
13	0.75	0.436	6.31	0.668	-6.91	No trend	No trend
14	0.99	0.534	6.13	0.751	-9.01	No trend	No trend
15	2.11	0.739	4.56	0.902	-13.28	Increasing trend	No trend
16	2.04	0.868	4.92	1.137	-17.60	Increasing trend	No trend
17	1.97	1.081	5.66	1.337	-20.81	Increasing trend	No trend
18	2.35	1.180	5.49	1.288	-19.97	Increasing trend	No trend
19	1.97	0.950	6.22	1.102	-15.54	Increasing trend	No trend
20	0.88	0.354	6.57	0.592	-5.13	No trend	No trend
21	0.44	0.153	6.39	0.319	0.06	No trend	No trend
22	0.99	0.318	6.20	0.439	-2.48	No trend	No trend
23	1.19	0.587	6.43	0.704	-7.52	No trend	No trend
24	1.12	0.616	5.99	0.617	-6.18	No trend	No trend
25	0.68	0.228	6.23	0.325	-0.22	No trend	No trend
26	-0.75	-0.291	6.11	-0.090	7.89	No trend	No trend
27	-1.36	-0.599	5.02	-0.395	12.81	No trend	No trend
28	-1.70	-0.896	5.18	-0.729	19.56	No trend	No trend
29	-1.29	-0.524	4.74	-0.452	13.66	No trend	No trend
30	-0.31	-0.138	3.92	-0.092	5.72	No trend	No trend
31	-1.60	-0.544	5.05	-0.540	15.75	No trend	No trend
32	-0.68	-0.167	4.41	-0.094	6.25	No trend	No trend
33	0.24	0.070	4.07	0.112	1.84	No trend	No trend

location 2. As the Sen's slope estimator, the mean H_{m0} shows a similar pattern in the slope of the linear best-fit curve (Table 2). Mean WS in this region has a maximum increasing trend of 0.813 cm/s/year at location 3 and a minimum increasing trend of 0.01 cm/s/year at location 9 as the slope of the linear best-fit curve (Table 4). The Mann–Kendall test shows a significant increasing trend at locations 2, 3, 5, and 6 for mean WS (Table 4) and location 2 for maximum WS (Table 5) at the 5 % significance level. At the 1 % significance level, a

Table 5 Long-term trends in annual maximum WS using Sen’s slope estimator and linear regression methods

Location	Test Z	Sen estimator		Linear regression		Trend	
		Q (cm/s)	B	Q (cm/s)	B	at $\alpha = 0.05$	at $\alpha = 0.01$
1	0.51	2.201	17.28	3.042	-42.91	No trend	No trend
2	2.79	8.947	12.42	9.873	-183.13	Increasing trend	Increasing trend
3	1.94	5.524	15.80	8.188	-146.58	No trend	No trend
4	0.65	2.574	13.84	3.129	-47.87	No trend	No trend
5	0.37	1.197	14.65	0.749	0.25	No trend	No trend
6	-0.71	-1.712	13.61	-1.556	44.80	No trend	No trend
7	-1.46	-3.507	14.35	-2.651	66.95	No trend	No trend
8	-0.63	-1.342	18.25	-0.691	32.44	No trend	No trend
9	-1.09	-3.316	16.24	-3.921	94.27	No trend	No trend
10	-0.51	-1.409	19.07	-0.888	36.45	No trend	No trend
11	-0.31	-1.359	19.87	-0.074	21.45	No trend	No trend
12	-0.07	-0.526	18.77	-0.397	26.88	No trend	No trend
13	-0.27	-2.019	20.17	-0.268	25.45	No trend	No trend
14	0.75	2.444	18.79	3.030	-42.09	No trend	No trend
15	-0.24	-0.965	16.54	0.627	4.26	No trend	No trend
16	-0.31	-1.182	17.80	1.147	-4.75	No trend	No trend
17	-0.41	-1.876	19.07	0.151	16.24	No trend	No trend
18	0.51	1.385	17.86	3.291	-46.71	No trend	No trend
19	0.00	0.007	18.81	2.594	-31.93	No trend	No trend
20	-0.48	-3.011	19.99	1.485	-9.50	No trend	No trend
21	-0.54	-2.293	19.22	0.506	9.06	No trend	No trend
22	-0.31	-1.052	18.79	0.591	7.14	No trend	No trend
23	-0.37	-1.933	20.35	-0.260	25.55	No trend	No trend
24	0.07	0.616	19.90	-0.791	36.07	No trend	No trend
25	0.03	0.044	21.13	-1.373	48.31	No trend	No trend
26	1.02	4.912	19.87	3.250	-43.87	No trend	No trend
27	0.37	1.712	16.88	-0.198	21.25	No trend	No trend
28	-0.48	-0.830	17.15	0.260	12.13	No trend	No trend
29	1.05	3.164	15.92	3.815	-59.78	No trend	No trend
30	1.22	4.031	13.04	3.704	-60.00	No trend	No trend
31	1.19	4.063	16.23	4.531	-73.20	No trend	No trend
32	0.75	2.729	15.44	3.412	-52.00	No trend	No trend
33	1.05	3.146	14.89	3.755	-59.43	No trend	No trend

significant increasing trend was observed at locations 3 and 5 for mean WS (Table 4) and location 2 for maximum WS (Table 5).

The long-term trend of wave climate in the north-eastern part (locations 11–16) of the Black Sea shows a weak but positive increasing trend except for maximum WS which has decreasing trend (Tables 2, 3, 4, 5). As the slope of the linear best-fit curve, trend of mean

H_{m0} decreases in value from location 11 (0.37 cm/year) to location 16 (0.161 cm/year). As the Mann–Kendall test in this region, all the locations show no trend except location 11 which shows significant increasing trend at the 5 % significance level in mean H_{m0} (Table 2), while maximum H_{m0} has no trend at all locations (Table 3). Mean WS in this region has an overall positive trend also, with an increasing pattern from location 12 (0.469 cm/s/year) to 16 (1.137 cm/s/year). Location 11 has the highest trend value of 1.219 cm/s/year in this region. The estimated trends in wind for these locations show significant increasing trend at the 5 % significance level for locations 15 and 16 in mean WS (Table 4) and no trend for all locations in maximum WS (Table 5).

In the north-western part (locations 18–24) of the Black Sea, long-term trend of wave climate also shows a positive increasing trend as the slope of the linear best-fit curve. The trend of mean H_{m0} decreases in value from location 18 (0.165 cm/year) to location 24 (0.01 cm/year) except for location 17 which has a positive increasing trend of 0.148 cm/year (Table 2). After applying the Mann–Kendall test in this region, it is seen that all the locations show no trend for both mean and maximum H_{m0} . The mean WS in this region has an overall positive trend, with high values at locations 17, 18 and 19 which are 1.337 cm/s/year, 1.288 cm/s/year, and 1.102 cm/s/year, respectively. The other locations have low wind speed trends with minimum value (0.319 cm/s/year) at location 21. The estimated trends in wind for these locations show significant increasing trend at the 5 % significance level for locations 17, 18 and 19 in mean WS (Table 4) and no trend for all locations in maximum WS (Table 5).

In the south-western part (locations 25–33) of the Black Sea, the annual mean H_{m0} varies from 0.68 to 1.02 m (Table 1), and annual maximum H_{m0} varies from 5.43 to 8.71 m. Annual mean WS varies from 6.27 to 3.88 m/s, while maximum WS varies from 25.93 to 17.25 m/s. As both slope estimators, mean H_{m0} has the significant decreasing trends at the 5 % significance level at locations 28 to 31 (Table 2), while no trend was observed at all locations in maximum H_{m0} (Table 3), mean WS (Table 4), and maximum

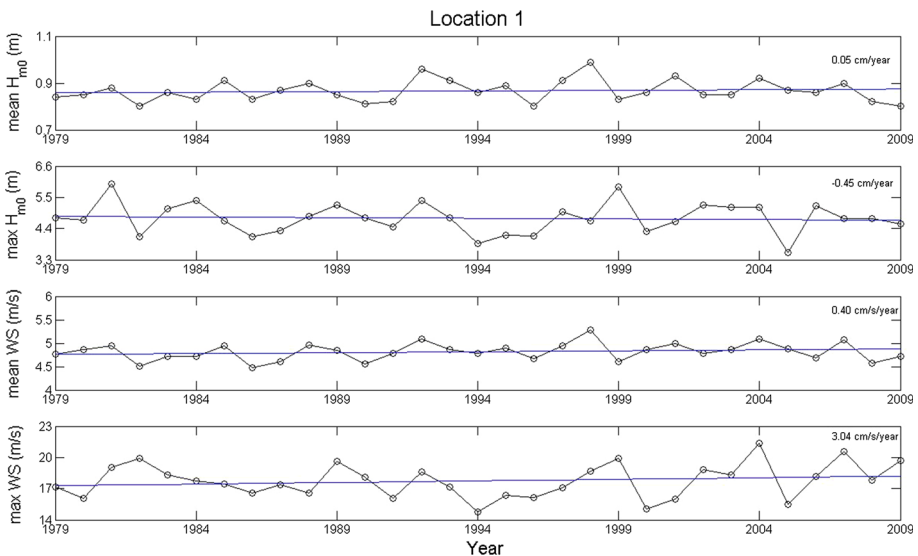


Fig. 7 Trends of annual mean and maximum H_{m0} and WS at location 1 during the period 1979–2009

WS (Table 5). Time series of annual mean and maximum H_{m0} and WS at location 1 during the period 1979–2009 are plotted in Fig. 7 as an illustration.

Finally, results of applying statistical tests for annual mean and maximum H_{m0} and WS over the period 1979–2009 show most of the significant trends at the 1 and 5 % significance levels for all variables were in no trend. On the annual time scale, the significant increasing trends were detected at the 5 % significance level at location 11 for mean H_{m0} , at locations 2, 3, 5, 6, 15, 16, 17, 18, and 19 for mean WS, and at location 2 for maximum WS. At the 1 % significance level, the significant increasing trends were detected at locations 3 and 5 for mean WS and location 2 for maximum WS. The significant decreasing trends were only detected at the 5 % significance level at locations 28–31 for mean H_{m0} . The rest locations have no significant trend at the both significance level for all variables. Spatial distribution of selected locations with increasing, decreasing, and no trends for the annual data series for four variables during the period 1979–2009 is presented in Fig. 8. As seen, in the north-western coasts of Turkey significant decreasing trends in mean H_{m0} dominate, while around Crimean Peninsula and in the north-eastern coasts of Turkey, significant increasing trends in mean WS dominate.

3.4 Decadal variation in annual mean and maximum H_{m0} and WS

Variations in the H_{m0} and WS in different decades are examined for the decadal periods the 1980s (1980–1989), 1990s (1990–1999), and 2000s (2000–2009). The mean and maximum values of the H_{m0} and WS during different decades for selected locations at different regions (south-eastern, north-eastern, north-western, south-western) over the Black Sea are computed and presented in Figs. 9 and 10. In the south-eastern region, the decadal

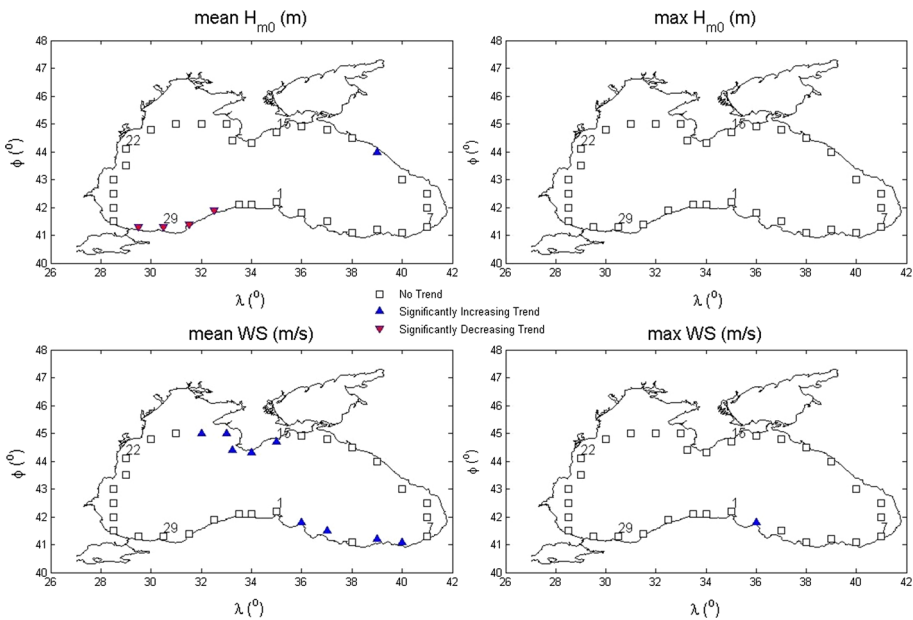


Fig. 8 Spatial distribution of selected locations with increasing, decreasing, and no trends by the Mann–Kendall and Sen’s tests at the 5 % significance level for the annual data series for four variables during the period 1979–2009

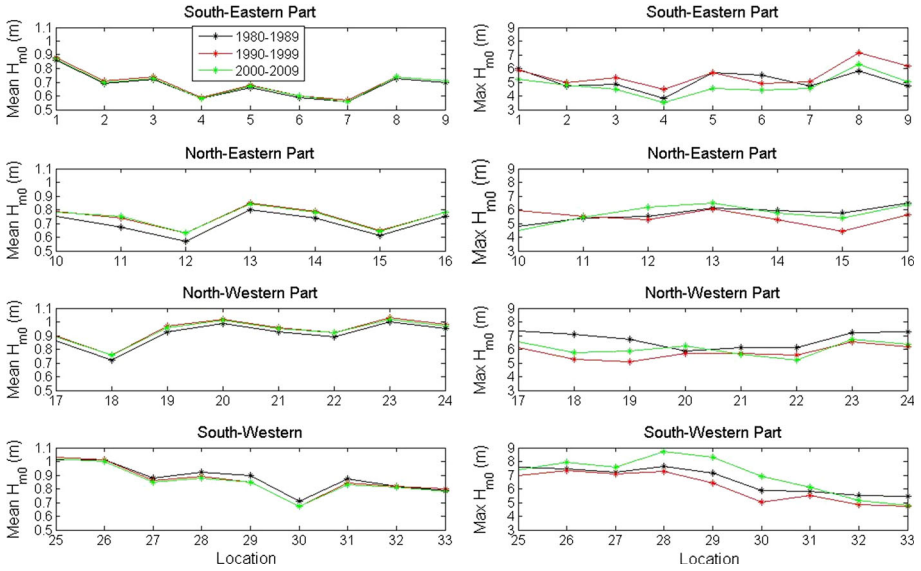


Fig. 9 Variation in mean (*left column*) and maximum (*right column*) H_{m0} computed from 31-year SWAN simulation in different decades at locations studied along the Black Sea shelves

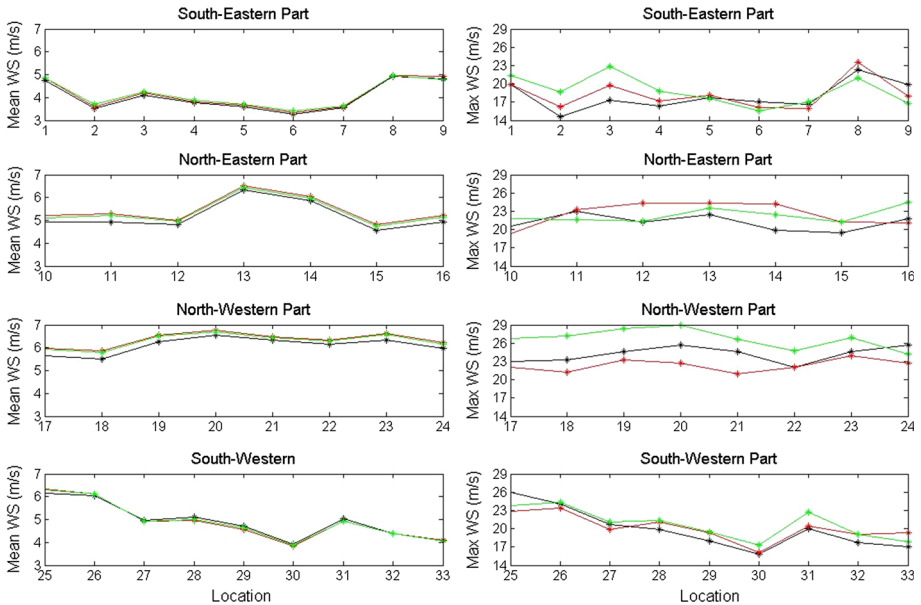


Fig. 10 Variation in mean (*left column*) and maximum (*right column*) WS computed from 31-year SWAN simulation in different decades at locations studied along the Black Sea shelves

variation in the mean H_{m0} is less than 0.1 m, and the variation in maximum H_{m0} in different decades is up to 1.44 m. The decadal variation in mean WS is less than 0.5 m/s, while the variation in maximum WS in different decades is up to 5.6 m/s. In the north-

eastern region, the decadal variations in the mean and maximum H_{m0} and mean WS are the same with that in the south-eastern region, while the variation, which is up to 4.23 m/s, in maximum WS in different decades is different. In the north-western region, the decadal variation in the mean H_{m0} is again less than 0.1 m, and the variation in maximum H_{m0} in different decades is up to 1.66 m. The decadal variation in mean WS is less than 0.5 m/s, while the variation in maximum WS in different decades is up to 6.14 m/s. In our fourth and last region, the south-western region, the decadal variation in the mean H_{m0} is again less than 0.1 m, and the variation in maximum H_{m0} in different decades is up to 1.86 m. The decadal variation in mean WS is less than 0.5 m/s, while the variation in maximum WS in different decades is up to 3.04 m/s. Based on the decadal variation results in different regions, we can conclude that there is a very low (almost negligible) variation in both the mean H_{m0} and WS, while the maximum H_{m0} and WS show high variations in different decades. This may be explained that the maximum H_{m0} and WS values are influenced by storms and cyclones, while the annual mean H_{m0} and WS values are barely influenced by such events.

4 Conclusions

This paper investigates a possible increase in the annual mean and maximum H_{m0} and WS from the 31-year long-term numerical simulations. This study was carried out by the application of the SWAN numerical model forced with the CFSR winds during the period of 1979 to 2009 over the Black Sea. The annual temporal and spatial variations of mean and maximum H_{m0} and WS were investigated. Based on the measured buoy data, validation of SWAN model results was carried out at four locations in the different parts of the Black Sea. The comparison statistics show that the simulation results match rather well with the measurements. Average of the correlation coefficient values was 0.91 and 0.85 for H_{m0} at four buoy locations and for T_{m02} at two buoy locations. The scatter index values for H_{m0} were 36, 49, 49, and 31 % at Gelendzhik, Hopa, Gloria, and Karaburun, respectively. On the other hand, these values for T_{m02} were 22 and 24 % at Gelendzhik and Hopa, respectively, while it was 31 % for T_p at Gloria.

Annual mean H_{m0} of surface wind waves generated in the computational domain without considering swell showed significant trend at 95 % confidence interval at the selected coastal locations of inner continental shelf (locations 28–31) of south-western part of the Black Sea and offshore Sochi (location 11) in the eastern part of the Black Sea during the simulated period. On the other hand, annual maximum H_{m0} showed no significant trend at all the selected locations. Annual mean WS of surface winds gave significant trend at 5 % significance level at the selected coastal locations of inner continental shelf (locations 2–6) of south-eastern part of the Black Sea and around inner continental shelf (locations 15–19) of the Crimean Peninsula in the northern part of the Black Sea during the simulated period. On the other hand, annual maximum WS showed significant trend only offshore Bafra (location 2) in the south-eastern of the Black Sea, and other all locations had no significant trend. The trends determined significantly for the winds or waves were observed at different locations, and thus at the same locations, the significant trends of winds do not match that of the waves. This may be due to effect of the swells, the prevailing wind direction in the area, and wave developing considering the wind direction. Therefore, individually analysis of wind–sea and swell parameters and directional analysis can be used to better understand the wave climate variability.

The highest difference in the mean H_{m0} between 1980–1989, 1990–1999, and 2000–2009 decades, more than 0.08 m at location 11, occurs at the selected locations of north-eastern part of the Black Sea, whereas the same region has the lowest difference in maximum H_{m0} . On the other hand, south-western part (1.86 m at location 30) shows the highest difference in maximum H_{m0} between the decades. The highest difference (6.14 m/s at location 20) in maximum WS between the decades occurs in the north-western part of the Black Sea, while it is 0.38 m/s at location 11 for mean WS. This shows that maximum H_{m0} and WS are influenced more than mean wind and wave conditions from the storm and cyclones cases.

Acknowledgments We would like to thank the NCEP CFS team for providing CFSR wind data, the NOAA (General Bathymetric Chart of the Oceans, GEBCO) for the providing the bathymetry data of the Black Sea, the Turkish Ministry of Transport (General Directorate of Railways, Ports and Airports Construction) for the providing the wave measurements at Karaburun, and the NIMRD (Oceanography Department) for the providing the wind and wave measurements at Gloria. The authors would like to acknowledge Prof. Dr. Erdal Özhan of the Middle East Technical University, Ankara, Turkey, who was the Director of the NATO TU-WAVES, for providing the buoy data at Gelendzhik, Hopa, and Sinop, and the NATO Science for Stability Program for supporting the NATO TU-WAVES project. We would also like to thank Dr Yalçın Yüksel for his contributions for the measurements at Karaburun and Dr Razvan Mateescu for his helps in providing the measurements at Gloria. This research was supported by the TUBITAK (The Scientific and Technological Research Council of Turkey) within a research project (Project code: 1001- Scientific and Technological Research Projects Funding Program, Project number: 214M436).

References

- Akpınar A, van Vledder GPh, Kömürçü Mİ, Özger M (2012) Evaluation of the numerical wave model (SWAN) for wave simulation in the Black Sea. *Cont Shelf Res* 50–51:80–99
- Akpınar A, Bekiroğlu S, van Vledder GPh, Bingölbali B (2015) Temporal and spatial analysis of wave energy potential during south western coasts of the Black Sea. TUBITAK Project No. 214M436
- Anoop TR, Kumar VS, Shanas PR, Glejin J (2015) Surface wave climatology and its variability in the North Indian Ocean based on ERA-Interim reanalysis. *J Atmos Ocean Technol* 32(7):1372–1385
- Bacon S, Carter DJT (1990) Wave climate changes in the North Atlantic and North Sea. *Int J Climatol* 11:45–558
- Battjes JA, Janssen JPFM (1978) Energy loss and set-up due to breaking of random waves. In: *Proceedings of 16th international conference on coastal engineering*, ASCE. pp 569–587
- Batu M (2008) Considering the condition of Karaburun sea with wave energy spectrum. Master thesis, Yıldız Technical University, Istanbul, Turkey (in Turkish)
- Booij N, Holthuijsen LH, Ris RC (1999) A third-generation wave model for coastal regions. Model description and validation. *J Geophys Res* 104(C4):7649–7666
- Caires S, Sterl A, Bidlot J-R, Graham N, Swail V (2004) Intercomparison of different wind-wave reanalysis. *J Climate* 17(10):1893–1913
- Çevik E, Yüksel Y, Yalçiner AC, Güler I, Ari A (2006) Determining shoreline change and sedimentation problem, case study: Karaburun, TÜBİTAK, İÇTAG 1845(1031008) (in Turkish)
- Cox A, Swail V (2001) A global wave hindcast over the period 1958–1997: validation and climate assessment. *J Geophys Res* 106(C2):2313–2329
- Dietrich JC, Zijlema M, Allier P-E, Holthuijsen LH, Booij N, Meixner JD, Proft JK, Dawson CN, Bender CJ, Naimaster A, Smith JM, Westerink JJ (2012) Limiters for spectral propagation velocities in SWAN. *Ocean Model* 70:85–102
- Douglas EM, Vogel RM, Kroll CN (2000) Trends in floods and low flows in the United States: impact of spatial correlation. *J Hydrol* 240:90–105
- Dragani WC, Martin PB, Simionato CG, Campos MI (2010) Are wind wave heights increasing in south-eastern south American continental shelf between 32°S and 40°S? *Cont Shelf Res* 30:481–490
- Eldeberky Y (1996) Nonlinear transformation of wave spectra in the nearshore zone, Ph.D. thesis, Delft University of Technology, The Netherlands

- GEBCO (2014) British Oceanographic Data Centre, Centenary Edition of the GEBCO Digital Atlas [CD-ROM]. Published on behalf of the Intergovernmental Oceanographic Commission and the International Hydrographic Organization, Liverpool
- Gorrell L, Raubenheimer B, Elgar S, Guza RT (2011) SWAN predictions of waves observed in shallow water onshore of complex bathymetry. *Coast Eng* 58:510–516
- Gower JFR (2002) Temperature, wind and wave climatologies, and trends from marine meteorological buoys in the northeast Pacific. *J Climate* 15:3709–3717
- Grevemeyer I, Herber R, Essen HH (2000) Microseismological evidence for a changing wave climate in the northeast Atlantic Ocean. *Nature* 408:349–352
- Gulev SK, Grigorieva V (2004) Last century changes in ocean wind wave height from global visual wave data. *Geophys Res Lett* 31:L24302
- Gulev SK, Hasse L (1999) Changes of wind waves in the North Atlantic over the last 30 years. *Int J Climatol* 19(10):1091–1117
- Hasselmann S, Hasselmann K, Allender JH, Barnett TP (1985) Computations and parameterizations of the linear energy transfer in a gravity wave spectrum, part II: parameterizations of the nonlinear transfer for application in wave models. *J Phys Oceanogr* 15(11):1378–1391
- Hithin NK, Kumar VS, Shanas PR (2015) Trends of wave height and period in the Central Arabian Sea from 1996 to 2012: a study based on satellite altimeter data. *Ocean Eng* 108:416–425
- Janssen PAEM (1989) Wave induced stress and the drag of air flow over sea waves. *J Phys Oceanogr* 19:745–754
- Janssen PAEM (1991) Quasi-linear theory of wind-wave generation applied to wave forecasting. *J Phys Oceanogr* 21:1631–1642
- Kendall MG (1975) Rank correlation methods. Griffin, London
- Komen GJ, Cavaleri L, Donelan M, Hasselmann K, Hasselmann S, Janssen PAEM (1994) Dynamics and modelling of ocean waves. Cambridge University Press, Cambridge, pp 554
- Krestenitis YN, Androulidakis Y, Kombiadou K (2012) Storm surge modelling in the Black Sea. In: Proceeding of protection and restoration of the environment XI, At Thessaloniki, Greece, pp 786–795
- Kumar VS, Anoop TR (2015) Spatial and temporal variations of wave height in shelf seas around India. *Nat Hazards* 78(3):1693–1706
- Kumar VS, Sajiv C (2010) Variations in long term wind speed during different decades in Arabian Sea and Bay of Bengal. *J Earth Syst Sci* 119:639–653
- Kumar D, Sannasiraj SA, Sundar V, Polnikov VG (2013) Wind wave characteristics and climate variability in the Indian Ocean region using altimeter data. *Mar Geod* 36:303–313
- Mann HB (1945) Nonparametric tests against trend. *Econometrica* 13:245–259
- Mendez FJ, Menendez M, Luceno A, Losada IJ (2006) Estimation of the long-term variability of extreme significant wave height using a time dependent POT model. *J Geophys Res* 111:C07024
- Menendez M, Mendez FJ, Losada IJ, Gram NE (2008) Variability of extreme wave heights in the north east Pacific Ocean based on buoy measurements. *Geophys Res Lett* 35:L22607
- Özhan E, Abdalla S (1998) Wind-wave climate of the Black Sea and the Turkish coast (NATO TU-WAVES project). Proceedings of 5th international workshop on wave hindcasting and forecasting, Jan 27–30, Melbourne, pp 71–82
- Özsoy E, Ünlüata Ü (1997) Oceanography of the Black Sea: a review of some recent results. *Earth-Sci Rev* 42:231–272
- Partal T, Kahya E (2006) Trend analysis in Turkish precipitation data. *Hydrol Process* 20:2011–2026
- Polonsky AB, Fomin VV, Garmashov AV (2011) Characteristics of wind waves of the Black Sea. *Rep Natl Acad Sci Ukr* 8:108–112 (Russian)
- Reguero BG, Méndez FJ, Losada IJ (2013) Variability of multivariate wave climate in Latin America and the Caribbean. *Global Planet Change* 100:70–84
- Ris RC, Holthuijsen LH, Booij N (1999) A third-generation wave model for coastal regions: 2, verification. *J Geophys Res* 104(C4):7667–7681
- Rogers WE, Hwang PA, Wang DW (2003) Investigation of wave growth and decay in the SWAN model: three regional-scale applications. *J Phys Oceanogr* 33:366–389
- Rusu E, Pilar P, Guedes Soares C (2008) Evaluation of the wave conditions in Madeira Archipelago with spectral models. *Ocean Eng* 35:1357–1371
- Saha S, Moorthi S, Pan H-L, Wu X, Wang J, Nadigai S, Tripp P, Kistler R, Woollen J, Behringer D, Liu H, Stokes D, Grumbine R, Gayno G, Wang J, Hou Y-T, Chuang H-Y, Juang H-MH, Sela J, Iredell M, Treadon R, Kleist D, van Delst P, Keyser D, Derber J, Ek M, Meng J, Wei H, Yang R, Lord S, van den Dool H, Kumar A, Wang W, Long C, Chelliah M, Xue Y, Huang B, Schemm J-K, Ebisuzaki W, Lin R, Xie P, Chen M, Zhou S, Higgins W, Zou C-Z, Liu Q, Chen Y, Han Y, Cucurull L, Reynolds RW,

- Rutledge G, Goldberg G (2010) The NCEP climate forecast system reanalysis. *B Am Meteorol Soc* 91:1015–1057
- Şahin C (2007) Parametric wind wave modelling; Western Black Sea case study. Master thesis, Yildiz Technical University, Istanbul, Turkey (in Turkish)
- Sajiv PC, Kumar VS, Glejin J, Dora GU, Vinayaraj P (2012) Interannual and seasonal variations in nearshore wave characteristics off Honnavar, west coast of India. *Curr Sci* 103:286–292
- Sen PK (1968) Estimates of the regression coefficient based on Kendall's tau. *J Am Stat Assoc* 63:1379–1389
- Shanas PR, Kumar VS (2015) Trends in surface wind speed and significant wave height as revealed by ERA-Interim wind wave hindcast in the Central Bay of Bengal. *Int J Climatol* 35:2654–2663
- Soares CG (1986) Assessment of the uncertainty in visual observations of wave height. *Ocean Eng* 13:37–56
- Sterl A, Komen GJ, Cotton P (1998) Fifteen years of global wave hindcasts using winds from ECMR weather forecast reanalysis: validating the reanalyzed winds and assessing the wave climate. *J Geophys Res* 103(C3):5477–5492
- Swain J (1997) Simulation of wave climate for the Arabian Sea and Bay of Bengal, PhD thesis, Naval Physical and Oceanographic Laboratory, Kochi
- Tabari H, Marofi S (2011) Changes of pan evaporation in the west of Iran. *Water Resour Manage* 25:97–111
- Tabari H, Marofi S, Aein A, Hosseinzadeh Talaei P, Mohammadi K (2011) Trend analysis of reference evapotranspiration in the western half of Iran. *Agric For Meteorol* 151(2):128–136
- Valchev NN, Trifonova EV, Andreeva NK (2012) Past and recent trends in the western Black Sea storminess. *Nat Hazards Earth Syst Sci* 12:961–977
- Van Ledden M, Vaughn G, Lansen J, Wiersma F, Amsterdam M (2009) Extreme wave event along the Guyana coastline in October 2005. *Cont Shelf Res* 29:352–361
- Van Vledder GPh, Akpınar A (2015) Wave model predictions in the Black Sea: sensitivity to wind fields. *Appl Ocean Res* 53:161–178
- Vanem E, Walker S-E (2013) Identifying trends in the ocean wave climate by time series analyses of significant wave height data. *Ocean Eng* 61:148–160
- Wang A, Swail V (2001) Changes of extreme wave heights in Northern Hemisphere Oceans and related atmospheric circulation regimes. *J Clim* 14(10):2204–2221
- Wang XL, Swail VR (2002) Trends of Atlantic wave extremes as simulated in a 40-yr wave hindcast using kinematically reanalyzed wind fields. *J Clim* 15(9):1020–1035
- WASA Group (1998) Changing waves and storms in the Northeast Atlantic? *Bull Am Meteorol Soc* 79:741–760
- Wolf J, Woolf DK (2006) Waves and climate change in the north-east Atlantic. *Geophys Res Lett* 33:L06604
- Woolf DK, Challenor PG, Cotton PD (2002) Variability and predictability of the North Atlantic wave climate. *J Geophys Res* 107(C10):3145
- Yue S, Hashino M (2003) Temperature trends in Japan: 1900–1996. *Theor Appl Climatol* 75:15–27
- Zijlema M (2010) Computation of wind-wave spectra in coastal waters with SWAN on unstructured grids. *Coast Eng* 57:267–277
- Zijlema M, Van Vledder GPh, Holthuijsen LH (2012) Bottom friction and wind drag for wave models. *Coast Eng* 65:19–26